

Climate impacts on multidecadal pCO₂ variability in the North Atlantic: 1948-2009

Melissa L. Breeden* and Galen A. McKinley

Department of Atmospheric and Oceanic Sciences, University of Wisconsin, Madison,
Wisconsin, USA

*Corresponding author: mbreeden@wisc.edu; 1225 W. Dayton St. Madison, WI 53706

Abstract

The North Atlantic is the most intense region of ocean CO₂ uptake in term of units per area. Here, we investigate multidecadal timescale variability of the partial pressure CO₂ (pCO₂) that is due to the natural carbon cycle using a regional model forced with realistic climate and pre-industrial atmospheric pCO₂ for 1948-2009. Large-scale patterns of natural pCO₂ variability are primarily associated with basin-averaged sea surface temperature (SST) that, in turn, is composed of two parts: the Atlantic Multidecadal Oscillation (AMO) and a long-term positive SST trend. The North Atlantic Oscillation (NAO) drives a secondary mode of variability. For the primary mode, positive AMO and the SST trend modify pCO₂ with different mechanisms and spatial patterns. Positive AMO is also associated with a significant reduction in dissolved inorganic carbon (DIC) in the subpolar gyre, due primarily to reduced vertical mixing; the net impact of positive AMO is to reduce pCO₂ in the subpolar gyre. Through direct impacts on SST, the net impacts of positive AMO is to increase pCO₂ in the subtropical gyre. From 1980 to present, long-term SST warming has amplified AMO impacts on pCO₂.

1 **1 Introduction**

2 To date, the ocean has removed approximately 1/3 of all anthropogenic carbon emitted to
3 the atmosphere and has, thus, substantially damped climate warming (Khatiwala et al., 2009;
4 Sabine et al., 2004). As carbon dioxide emissions continue to increase due to fossil fuel
5 emissions and cement production, there is significant interest in better understanding the ocean
6 carbon cycle. Due to the limited instrumental record and sparse data, multidecadal variability of
7 the ocean carbon sink remains poorly constrained. The North Atlantic, in particular, is a region
8 of highly concentrated carbon uptake (Takahashi et al., 2009) and of significant carbon cycle
9 variability related to variations in the climate, with multiple studies finding an association with
10 the North Atlantic Oscillation (Fay and McKinley, 2013; Schuster et al., 2013; Terry, 2012;
11 McKinley et al., 2011; Loptien and Eden, 2010; Ullman et al., 2009; Thomas et al., 2008).
12 However, data are sparse, processes are complex and the timescales for studies have differed,
13 and this has complicated a clear elucidation of the mechanisms of North Atlantic carbon cycle
14 variations.

15 Schuster et al. (2009) analyzed in situ pCO₂ measurements, and suggested a substantial
16 decline in North Atlantic carbon uptake from the mid-1990's to the mid-2000's. LeQuéré et al.
17 (2010) also interpreted observations and models to conclude that there had been a decline in the
18 North Atlantic sink from 1981-2007 due to changing wind patterns and increasing SST. Metzl et
19 al. (2010) focused on subpolar surface ocean carbon cycle changes between 1993-2008, and also
20 concluded that there had been a reduction in carbon uptake. In situ pCO₂ measurements have
21 also been synthesized to illustrate the strong sensitivities of such changes to the locations and
22 timeframe for the analyses (Fay and McKinley 2013; McKinley et al., 2011). The substantial
23 spatial heterogeneity and temporal variability in the North Atlantic complicates efforts to use
24 sparse observations to quantify carbon uptake. Thus, the magnitude and mechanisms North
25 Atlantic carbon cycle variability remains loosely constrained. The present study takes advantage
26 of the full spatial and temporal coverage of a regional numerical model to gain new insights into
27 the mechanisms of variability of North Atlantic pCO₂.

28 As shown by Ullman et al. (2009) in a 15-year simulation (1992-2006), internal
29 variability in the North Atlantic is partially obscured by the large, quasilinear trend of CO₂ flux
30 into the ocean that is driven by increasing CO₂ emissions. To examine the carbon sink variability
31 that is partially masked by this large carbon influx, we use a hindcast model from 1948-2009

1 forced with the preindustrial atmospheric CO₂ concentration and realistic climate. As described
2 below, we find that the basin-average SST is associated with the leading mode of surface ocean
3 pCO₂ variability. This SST signal, in turn, includes an upward trend due to greenhouse gas
4 emissions and a signal of internal variability characterized by the Atlantic Multidecadal
5 Oscillation (AMO, Kerr, 2000).

6 **2 Methodology**

7 **2.1 Physical-Biogeochemical-Ecosystem Model**

8 The MIT Ocean General Circulation Model (Marshall et al., 1997a, 1997b) has been
9 regionally configured for the North Atlantic between 20°S and 81.5°N (Bennington et al., 2009;
10 Ullman et al., 2009). The model has a horizontal resolution of 0.5° latitude and 0.5° longitude
11 and 23 vertical levels beginning with a resolution of 10m thickness at the surface and increasing
12 to 500 m thickness at depths greater than 2200 m. The Gent-McWilliams (Gent and McWilliams,
13 1990) eddy parameterization and the KPP boundary layer mixing scheme (Large et al., 1994)
14 were employed to model sub-grid-scale processes. Daily fields from NCEP/NCAR Reanalysis I
15 force the model from 1948-2009 (Kalnay et al., 1996). SST and SSS are relaxed to monthly
16 historical SST (Had1SSTv1.0, Rayner et al., 2003) and climatological SSS (Antonov et al.,
17 2006) observations, on the timescale of two and four weeks, respectively. Glacier melt and/or
18 river discharge are not included in the model forcing, instead the SSS relaxation approximates
19 these impacts. [Freshwater \(evaporation – precipitation\) forcing and SSS relaxation impacts both](#)
20 [salinity and tracer concentrations. In lieu of an active sea ice simulation, observed fractional ice](#)
21 [from NCEP Reanalysis 1 is applied with interpolation to daily resolution.](#)

22 For open boundary conditions, a sponge layer exists at 20S, and over the first 5 degrees of
23 latitude to the North, there is restoration to climatological temperature, salinity, DIC and
24 phosphate fields. For temperature and salinity, there is also a sponge layer at Gibraltar. More
25 discussion of the sponge layer can be found in Ullman et al., 2009.

26 The pelagic ecosystem is parameterized using one zooplankton class and two
27 phytoplankton classes (diatoms and ‘small’ phytoplankton) as described previously (Dutkiewicz
28 et al., 2005; Bennington et al., 2009; Ullman et al., 2009). Carbon (inorganic and dissolved and
29 particulate organic), alkalinity (ALK), phosphorus, silica and iron cycling are explicitly included
30 in the biogeochemical model. Carbonate chemistry is modeled as in Follows et al. (2006). The
31 objective of this simulation is to identify climate impacts on the natural carbon cycle without the

1 complication of the large CO₂ flux into the ocean that is observed. Thus, atmospheric pCO₂ is
2 fixed at a constant, preindustrial level of 278 ppmv.

3 The physical model was spun up for 100 years. Following the physical spinup, the
4 biogeochemical model was initialized using preindustrial estimates for DIC and ALK
5 climatology from the GLODAP database (Key et al., 2004). The biogeochemical model was
6 then spun up for an additional 100 years, long enough to eliminate drift in the biogeochemical
7 parameters. The percent change over the last five years of spinup in the basin-averaged surface
8 DIC field is 0.00046% per year. For comparison, the percent change in DIC from a high AMO
9 (1955) to low AMO (1975) is .012% per year, two orders of magnitude greater than drift at the
10 end of the spin up. This indicates that a 100-year biogeochemical spinup is sufficient to
11 eliminate model drift that would impact our upper ocean analysis. Following spinup, the model
12 was then run with NCEP/NCAR daily forcing fields for 1948-2009.

13 Model physics across the North Atlantic, as well as pCO₂, DIC and ALK at the Bermuda
14 Atlantic Time Series (Bates, 2007) and in the subpolar North Atlantic have been compared to
15 results from a previous simulation using with this same model forced with observed atmospheric
16 pCO₂ for 1992-2006 (Ullman et al., 2009). Comparison of this simulation to estimates of the pre-
17 industrial vertical profile of DIC in the subpolar gyre indicates good performance by the model
18 (Supplementary Figure 1 and text). Mikaloff-Fletcher et al. (2007) estimated the pre-industrial,
19 or ‘natural’, air-to-sea CO₂ flux in the North Atlantic with an ocean inversion that incorporated
20 climatological circulations estimated from 10 ocean circulation models. For the North Atlantic
21 from 0° to 75°N, they find an uptake of 0.27±0.07 PgC/yr. The mean natural CO₂ flux averaged
22 over the same spatial domain in our simulation is consistent, 0.23 PgC/yr. In total, our
23 comparison to available data indicate that the model is capable of robustly simulating the carbon
24 biogeochemistry of the North Atlantic and its response to climate variability.

25 **2.2 Post-processing**

26 CO₂ flux into the ocean is proportional to the partial pressure difference between the
27 atmosphere and ocean surface: $\Delta p\text{CO}_2 = p\text{CO}_2^{\text{atm}} - p\text{CO}_2^{\text{ocn}}$. In this analysis, we can directly
28 relate higher pCO₂^{ocn} to a reduction in CO₂ flux, since atmospheric pCO₂ is fixed. $\Delta p\text{CO}_2$
29 variability sets the sign and magnitude of flux changes on both seasonal and interannual
30 timescales (Takahashi et al. 2009, Watson et al. 2009, LeQuéré et al. 2010). pCO₂ is
31 decomposed into contributions from temperature and chemical effects using model output and

1 the full carbonate equations (Follows et al., 2006). As in Ullman et al. (2009), pCO₂-SST is
2 found by allowing only SST to vary in the full carbonate equations for pCO₂, i.e. all other
3 variables (DIC, ALK, SSS, phosphate, silica) are held constant at their long-term mean values;
4 pCO₂-chem is found by holding SST constant and allowing the rest of the input variables to vary;
5 for pCO₂-DIC, only DIC varies.

6 Model diagnostics for DIC are the monthly mean tendency terms (in mmol/m³/yr) due to
7 individual modeled processes and are calculated at each time step during the model simulation
8 (Ullman et al., 2009). Monthly mean diagnostics for the surface layer DIC change due to
9 horizontal and vertical advection and diffusion, net biological processes (primary production and
10 respiration), freshwater input/removal, and air-sea CO₂ flux are used.

11 The AMO index for the model is calculated using modeled SST and observed global
12 Had1SSTv1.0 (Rayner et al., 2003) using the approach of Wang and Dong (2010). This
13 approach regresses the area-weighted global mean Had1SST time series onto area-weighted
14 basin-wide mean North Atlantic SST time series (NASST). This regressed index is subtracted
15 from the total NASST to define the AMO. The combined SST signal is, thus, decomposed into
16 contributions from globally increasing SST (SST trend) and the internal variability of the AMO
17 (Figure 1d). In order to focus on the decadal timescale variability, all timeseries are smoothed
18 with a standardized 121-month box smoother.

19 **3 Results**

20 **3.1 Multidecadal Variability**

21 To determine the leading mode of variability in surface ocean pCO₂, principle component
22 analysis is employed. The first empirical orthogonal function (EOF1) patterns and smoothed
23 principle components (PCs) for monthly, 13-month smoothed total pCO₂ and the SST
24 contribution to pCO₂ (pCO₂-SST) are shown in Figure 1a-c. To determine the change in pCO₂
25 anomalies described by EOF1 at a specific point in time, the value of the PC1 at that time can be
26 multiplied by the EOF1 pattern. The percent of variance in the total field explained by the EOF1
27 pattern is 18% and 38% for pCO₂ and pCO₂-SST, respectively. In both cases, the EOF1 patterns
28 are statistically distinct from their EOF2 patterns, which are discussed in section 4. This EOF
29 analysis unveils the basin-scale coherent variability. There is remaining variability in coherent
30 secondary large-scale modes (e.g. EOF2) or at scales smaller than the whole basin. That large-
31 scale modes of climatic variability tend to capture 10-40% of variance has been documented

1 across many climate variables, including global SST and tropospheric winds (von Storch and
2 Zwiers, 1999), Southern Ocean geopotential heights (Thomson and Wallace, 2000), and pCO₂
3 throughout the Pacific (McKinley et al. 2004, 2006). That pCO₂ EOF1 captures the patterns of
4 multi-decadal large-scale change is further evidenced by plots of 20-year anomalies of pCO₂ ,
5 (Figure S2).

6 The correlation between PC1-pCO₂ and the area-weighted basin-averaged SST is 0.88
7 (Figure 1c, Table S1). An increase in temperature increases pCO₂ by reducing solubility, which
8 is illustrated by the pCO₂-SST EOF1 pattern. PC1- pCO₂ and PC1- pCO₂-SST are highly
9 correlated (Figure 1c, $r = 0.91$), but have distinct EOF1 patterns, particularly in the subpolar gyre
10 (Figure 1a,b). This is consistent with the pCO₂ in the subpolar gyre also being significantly
11 impacted by changes in DIC supply which in turn, are associated with the AMO. EOF1 for
12 pCO₂-chem and pCO₂-DIC explain 32% and 25% of the variance, respectively (Figure 2a,b), and
13 these PC1's are highly correlated with the AMO, $r = 0.99, 0.96$, respectively (Figure 2d, Table
14 S1).

15 Alkalinity can also affect pCO₂-chem since increased alkalinity reduces pCO₂. PC1 for
16 EOF1 of pCO₂-ALK (Figure 2c) does not correlate highly to PC1's of total pCO₂ or pCO₂-chem
17 ($r = -0.25$; $r = 0.44$, respectively), or to the AMO (see supplementary table 1). Though alkalinity
18 does contribute to the spatial pattern shown in the EOF1 of pCO₂-chem, the temporal evolution
19 of this pattern differs substantially and is not strongly connected to the AMO or to EOF1 of
20 pCO₂. Therefore, we focus on the more direct relationship between pCO₂-DIC and pCO₂-chem
21 for the rest of the paper, and reserve the alkalinity relationships for future in-depth analysis.

22 The AMO, an index of internal North Atlantic SST variability, declines (cools) until 1975
23 and rises thereafter (Figure 1d). Taking the last half of the timeseries as an example, increasingly
24 positive AMO corresponds to a decrease in pCO₂-chem, with the strongest declines in the
25 subpolar gyre and driven by reduced pCO₂-DIC (Figure 2). This occurs in opposition to the
26 direct effect on pCO₂ of warmer NASST (Figure 1b,c), driven jointly by the increasingly positive
27 AMO and the warming trend (Figure 1d). SST and chemical terms vary inversely because higher
28 SST enhances stratification, leading to a shoaling of mixed layer depths over most of the gyre
29 (Figure S2). This shoaling in turn limits the amount of deep, carbon-rich water that is mixed to
30 the surface, reducing pCO₂-DIC and pCO₂-chem (Ullman et al., 2009). The correlation of PC1-

pCO₂-chem and PC1-pCO₂-DIC with PC1-pCO₂-SST are 0.90 and 0.91, respectively (Table S1). Mechanisms of AMO impacts on pCO₂-chem in the subpolar gyre will be explored further below.

3.2 Regression Analysis

Regression of the AMO, SST trend, and total SST (Figure 1d) onto monthly pCO₂, pCO₂-SST and pCO₂-chem further illustrates that temperature and chemical responses tend to act in opposition to one another, damping total pCO₂ responses across the basin (Figure 3). This analysis compliments the above EOF analysis by allowing the use of the same index of temporal variability across all fields. Previous studies with observations and models have shown that pCO₂-chem dominates the seasonality of pCO₂ in the subpolar gyre, via strong vertical supply of DIC in winter that drives up pCO₂ and biological DIC drawdown in summer that drives pCO₂ down. Temperature impacts oppose these seasonal oscillations, but are of weaker amplitude (Kortzinger et al. 2008; Takahashi et al. 2002). Models have shown similar opposing influences with respect to interannual variability (Ullman et al. 2009; McKinley et al. 2004). These regressions illustrate that positive AMO leads to higher pCO₂-SST throughout the basin (Figure 3b). The response is strongest north of 35°N with a clear maximum to the east of Newfoundland. Simultaneously, positive AMO is associated with a reduction in pCO₂-chem (Figure 3c). The pCO₂-chem signal is also strongest to the north. The overall effect is a decrease in total pCO₂ north of 45°N and a slight increase in pCO₂ in the eastern subtropical gyre (Figure 3a).

When responding to the global SST trend, pCO₂-SST more heavily controls the response of the total pCO₂ field (Figure 3d,e). The pCO₂-SST response is strongest along the Gulf Stream and east of Newfoundland, and also increases somewhat off the coast of Europe and Africa. pCO₂-chem exhibits some decline in the Gulf Stream region, and has a small response elsewhere (Figure 3f).

Regression with the total NASST timeseries (Figure 1) illustrates the combined effects of the AMO and trend signals (Figure 3g-i). A positive anomaly of NASST depresses total pCO₂ in the subpolar gyre, consistent with the AMO impact found above. Positive NASST also increases total pCO₂ off North Africa, consistent with the impact of the SST trend. pCO₂-SST increases both off Africa and has a strong maximum in the Gulf Stream region east of Newfoundland with positive NASST anomalies. The pCO₂-chem response is slightly weaker in the subpolar gyre than for the AMO alone (Figure 3a,i).

3.3 DIC Diagnostics

1 To further investigate the chemical term response to the AMO, model diagnostics for the
2 DIC field are regressed upon the AMO index. Diagnostics are modeled rates of change in DIC
3 due to one of five processes that have been saved at every model time-step. Physical processes
4 are separated into horizontal advection and diffusion (DIC-horz), and vertical advection and
5 diffusion (DIC-vert). DIC-phys is the sum of vertical and horizontal transport, showing the net
6 effect of physical transport on DIC (Figure 4). The rate of DIC supply is also affected by
7 biological processes involving DIC incorporation into organic matter and remineralization back
8 to inorganic (DIC-bio), net precipitation/evaporation that dilutes or concentrates DIC (DIC-
9 fresh) and the air-sea flux of CO₂ (DIC-flx) (Figure 5). The focus on DIC is justified by the fact
10 that pCO₂-chem change has the same pattern and is highly correlated with pCO₂-DIC change
11 (Figure 2). The focus on the AMO is justified by its strong imprint on pCO₂ through pCO₂-chem
12 (Figure 2, 3).

13 For the long-term average, vertical advection and diffusion are positive along the Gulf
14 Stream and in the subpolar gyre due to deep winter mixed layer depths (MLD) that mix up high-
15 DIC water from below (Figure 4a). Horizontal DIC advection and mixing removes this vertically
16 supplied DIC along the Gulf Stream and in the western subpolar gyre (Figure 4b). While the
17 vertical and horizontal components tend to have opposing influences, the net effect is a positive
18 DIC supply to the subpolar gyre, as shown by mean DIC-phys (Figure 4c). With positive AMO,
19 vertical advective and diffusive fluxes of DIC decrease in the Irminger Sea and Iceland basin,
20 while they increase in the Labrador Sea and east of Newfoundland (Figure 4d). These changes
21 are consistent with AMO-related MLD changes outside of the Labrador Sea (Figure 5) and
22 change in the basin-scale barotropic streamfunction indicating a weakened subpolar gyre (Figure
23 6). The effect of this is to shift the central DIC-vert maximum to the west. With positive AMO,
24 horizontal advection and diffusion largely respond to changes in vertical advection and diffusion,
25 with less horizontal divergence (a positive change) in regions where the vertical supply is
26 reduced (Figure 4e). The net effect shown by DIC-phys reveals an overall reduction in DIC
27 supply (Figure 4f), consistent with a weaker subpolar gyre circulation and shallower MLDs that
28 reduce the vertical supply of DIC. Hakkinen and Rhines (2009) illustrate and increased
29 penetration of subtropical waters into the subpolar region from the 1990s to the 2000s, consistent
30 with a weaker subpolar gyre circulation. The changes in MLD and streamfunction are also in
31 agreement with results from Zhang (2008) who links the observed spindown of the subpolar gyre

1 in the 1990's to an enhanced MOC using a combination of satellite altimeter observations and
2 results from a 1000-year coupled ocean-atmosphere model simulation.

3 Mean DIC impacts from physics, biological processes, freshwater and air-sea flux are
4 shown in Figure 7a-e. The net impact of biology is to remove DIC from the surface of most of
5 the region, with the most intense removal along the Gulf Stream (Figure 7a). The smaller impact
6 of evaporation and precipitation is to concentrate DIC in the subtropics and to dilute it in the
7 subpolar gyre (Figure 7b). The air-sea CO₂ flux term is also small, positive north of about 35°N
8 and negative to the south (Figure 7c). AMO-related change in the biological removal of DIC
9 indicates additional removal (negative anomaly) occurring in the same region where horizontal
10 flux increases, consistent with biological stimulation through an increased supply nutrients from
11 the subtropical subsurface along the “nutrient stream” (Williams et al., 2006). There is reduced
12 biological productivity, and thus a reduction of DIC loss (a positive DIC anomaly), in other parts
13 of the basin that are consistent with satellite observations from the late 1990s to the mid-2000s
14 (Behrenfeld et al. 2006). Changes in surface ocean DIC content due to freshwater fluxes and air-
15 sea CO₂ flux with the AMO are small. Across the basin, the net DIC change associated with
16 AMO is negative, with the strongest negative changes occurring in the subpolar gyre (Figure 2b,
17 3c)

18 **4 Discussion and Conclusions**

19 In this North Atlantic regional model forced with pre-industrial pCO₂ and realistic
20 climate from 1948-2009, SST is the dominant driver of pCO₂ variability, with both long-term
21 anthropogenic warming and the AMO playing important roles. The AMO strongly influences
22 chemical change, which in turn is mostly driven by DIC. DIC changes, in turn, are due primarily
23 to changes in vertical and horizontal advection and mixing. Changing biology has the most
24 important secondary effect, and largely damps the anomalies caused by advection and mixing.
25 Freshwater and CO₂ fluxes changes are slight.

26 Our findings linking the AMO to natural carbon cycle variability in the North Atlantic are
27 consistent with the study of Séférian et al. (2013) who also found an AMO-like signal dominated
28 North Atlantic pCO₂ variability in a 1000-year Earth System Model simulation with constant
29 pCO₂. Other studies have focused on the relationship between the North Atlantic Oscillation
30 (NAO) and CO₂ flux using models and observations (Loptien and Eden 2010; Ullman et al.
31 2009; Schuster et al., 2009; Thomas et al., 2008). Consistent with these previous studies, the

1 NAO is the second mode of variability in this simulation (Figure S4, S5), and the corresponding
2 principle components are highly correlated with the NAO (Table S2). The shorter timeframe for
3 most previous studies explains, in part, the difference in attribution to the AMO as opposed to
4 NAO. Our results are broadly consistent with previous studies in the finding that physical
5 variability is the dominant driver of variability in the North Atlantic surface ocean carbon cycle.

6 The NAO and AMO may, in fact, be linked through the Meridional Overturning
7 Circulation (MOC), with a positive NAO enhancing MOC, which over time warms SSTs and
8 leads to a positive AMO. The precise mechanisms remain in debate due to different model
9 findings and a lack of observational constraints (Delworth & Mann, 2000; Knight et al., 2005;
10 Dima & Lohmann, 2007; Latif et al., 2006). In this simulation, the NAO and MOC are
11 significantly correlated ($r = 0.57$, Table S1) and there is also a high correlation ($r = 0.86$)
12 between the NAO (Figure S3) and the 15-year lagged AMO. These correlations are consistent
13 with the above-postulated NAO-MOC-AMO relationship. On the other hand, Booth et al. (2012)
14 suggest that the AMO may be driven, in fact, by atmospheric aerosol variability, so it is possible
15 that there is no direct AMO-MOC relationship. Future modeling and observations should further
16 elucidate these connections.

17 We find multidecadal variability in the natural carbon cycle of the surface North Atlantic
18 to be dominated by the SST trend and multidecadal SST variation captured by the AMO index.
19 Variability linked to AMO influences both $p\text{CO}_2$ -SST and $p\text{CO}_2$ -chem. In the subpolar gyre, the
20 positive SST influence on $p\text{CO}_2$ is overwhelmed by reduced supply of DIC to the surface ocean
21 through mixing and advection, the net impact being reduced $p\text{CO}_2$. The reduction in mixing is
22 associated with shoaling of MLDs and a weaker subpolar gyre circulation, both associated with
23 warmer SSTs (positive AMO). In the subtropics, the SST impact is stronger and thus $p\text{CO}_2$ is
24 increased under the influence of positive AMO and positive SST trend.

25 These findings are consistent with observed relationships between trends in surface ocean
26 $p\text{CO}_2$ and trends in atmospheric $p\text{CO}_2$ since the 1980s (Fay and McKinley, 2013). In the North
27 Atlantic subpolar gyre, trends in surface ocean $p\text{CO}_2$ lagged the trend in atmospheric $p\text{CO}_2$ from
28 the early to mid 1990s to the late 2000s, which is consistent with the AMO and the SST trend
29 reducing DIC supply to the subpolar gyre as found in this study. On smaller spatial scales and
30 shorter timeframes, trends in ocean $p\text{CO}_2$ can differ (Fay and McKinley, 2013; Metzl 2010,
31 Watson et al 2009, Schuster et al. 2009), which can be reasonably attributed to shorter-term and

smaller spatial scale variability. We also find that warming has contributed to the observed pCO₂ increase from the 1980-90s through the 2000s throughout the basin. These model results allow a mechanistic attribution of these observed changes in North Atlantic pCO₂ to the combined effect of the AMO and a positive SST trend due to anthropogenic climate change.

Acknowledgements

The authors are grateful for support from NASA grants (NNX/11AF53G, and NNX/13AC53G). Model code is freely available at MITgcm.org; model fields analyzed here can be acquired by contacting GAM.

References

- Antonov, J. I., R. A. Locarnini, T. P. Boyer, A. V. Mishonov, and H. E. Garcia (2006), World Ocean Atlas 2005 vol. 2, Salinity, NOAA Atlas NESDIS 62, edited by S. Levitus, 182 pp., U.S. Govt. Print. Off., Washington, D. C..
- Bates, N. R (2007), Interannual variability of the oceanic CO₂ sink in the subtropical gyre of the North Atlantic Ocean over the last 2 decades, *J. Geophys. Res.*, 112, C09013, doi:10.1029/2006JC003759.
- Behrenfeld, M. J., R. T. O'Malley, D. A. Siegel, C. R. McClain, J. L. Sarmiento, G. C. Feldman, A. J. Milligan, P.G. Falkowski, R. M. Letelier, E. S. Boss (2006), Climate-driven trends in contemporary ocean productivity. *Nature* **444**, 752–755.
- Bennington, V., G. A. McKinley, S. Dutkiewicz, and D. Ullman (2009), What does chlorophyll variability tell us about export and CO₂ flux variability in the North Atlantic?, *Global Biogeochem. Cycles*, 23, GB3002, doi:10.1029/2008GB003241.
- Booth, B. B. B., N. J. Dunstone, P. R. Halloran, T. Andrews, N. Bellouin (2012), Aerosols implicated as a prime driver of twentieth-century North Atlantic climate variability. *Nature*, **484**, 228-232, doi:10.1038/nature10946.
- Delworth, T. L., and M. E. Mann (2000), Observed and simulated multidecadal variability in the Northern Hemisphere, *Clim. Dyn.*, 16, 661–676, doi:10.1007/s003820000075.

- 1 Dima, M, and G. Lohmann (2007), A Hemispheric Mechanism for the Atlantic Multidecadal
2 Oscillation, *J. Climate*, 20, 2706-2718, DOI: 10.1175/JCLI4174.1.
- 3 Dutkiewicz, S., M. J. Follows, and P. Parekh (2005), Interactions of the iron and phosphorus
4 cycles: A three-dimensional model study, *Global Biogeochem. Cycles*, 19, GB1021,
5 doi:10.1029/2004GB002342.
- 6 Fay, A. R., and G. A. McKinley (2013), Global trends in surface ocean pCO₂ from in situ data,
7 *Global Biogeochem. Cycles*, 27, doi:10.1002/gbc.20051.
- 8 Follows, M. J., S. Dutkiewicz, and T. Ito (2006), On the solution of the carbonate system in
9 ocean biogeochemistry models, *Ocean Modell.*, 12, 290–301,
10 doi:10.1016/j.ocemod.2005.05.004.
- 11 Gent, P. R., and J. C. McWilliams (1990), Isopycnal mixing in ocean general circulation models ,
12 *J. Phys. Oceanogr.*, 20, 150–155.
- 13 Hakkinen, S., and P. B. Rhines (2009), Shifting surface currents in the northern North Atlantic
14 Ocean, *J. Geophys. Res.*, 114, C04005, doi:10.1029/2008JC004883.
- 15 Key, R. M., R. M. Key, A. Kozyr, C. L. Sabine, K. Lee, R. Wanninkhof, J. L. Bullister, R. A.
16 Feely, F. J. Millero, C. Mordy , T.-H. Peng (2004), A global ocean carbon climatology:
17 Results from Global Data Analysis Project (GLODAP), *Global Biogeochem. Cycles*, 18,
18 GB4031, doi:10.1029/2004GB002247.
- 19 Kalnay, E., M. Kanamitsu, R. Kistler, W. Collins, D. Deaven, L. Gandin, M. Iredell, S. Saha, G.
20 White, J. Woollen, Y. Zhu, A. Leetmaa, R. Reynolds, M. Chelliah, W. Ebisuzaki, W. Higgins,
21 J. Janowiak, K. C. Mo, C. Ropelewski, J. Wang, R. Jenne, and D. Joseph (1996), The
22 NCEP/NCAR 40-Year Reanalysis Project, *Bull. Amer. Meteor. Soc.*, 77, 437–471,
23 doi: [http://dx.doi.org/10.1175/1520-0477\(1996\)077<0437:TNYRP>2.0.CO;2](http://dx.doi.org/10.1175/1520-0477(1996)077<0437:TNYRP>2.0.CO;2).
24
- 25 Kerr, R. A. (2000), A North Atlantic Climate Pacemaker for the Centuries, *Science*, 288, 1984-
26 1985, doi:10.1126/science.288.5473.1984.
- 27

- 1 Khatiwala, S., F. Primeau, and T. Hall (2009), Reconstruction of the history of anthropogenic
2 CO₂ concentrations in the ocean, *Letters to Nature*, 462, 346-349, doi:10.1038/nature08526.
3
- 4 Knight, J. R., R. J. Allan, C. K. Folland, M. Vellinga, and M. E. Mann (2005), A signature of
5 persistent natural thermohaline circulation cycles in observed climate, *Geophys. Res. Lett.*,
6 32, L20708, doi:10.1029/ 2005GL024233.
- 7 Körtzinger, A., U. Send, R. S. Lampitt, S. Hartman, D. W. R. Wallace, J. Karstensen, M. G.
8 Villagarcia, O. Llinás, and M. D. DeGrandpre (2008) The seasonal pCO₂ cycle at
9 49°N/16.5°W in the northeastern Atlantic Ocean and what it tells us about biological
10 productivity. *J. Geophys. Res* **113**, C04020.
- 11 Large, W. G., J. C. McWilliams, and S. C. Doney (1994), Oceanic vertical mixing: A review and
12 a model with a nonlocal boundary layer parameterization, *Rev. Geophys.*, 32, 363–403.
- 13 Latif, M., C. Böning, J. Willebrand, A. Biastoch, J. Dengg, N. Keenlyside, U. Schweckendiek,
14 and G. Madec (2006), Is the Thermohaline Circulation Changing?, *J. Climate*, 19, 4631–4637,
15 doi: <http://dx.doi.org/10.1175/JCLI3876.1>
16
- 17 Le Quéré, C., Takahashi, T., Buitenhuis, E. T., Rödenbeck, C. & Sutherland, S. C. (2010),
18 Impact of climate change and variability on the global oceanic sink of CO₂, *Global*
19 *Biogeochem Cycles*, 24, GB4007, doi: 10.1029/2009GB003599.
20
- 21 Löptien, U., and C. Eden (2010), Multidecadal CO₂ uptake variability of the North Atlantic, *J.*
22 *Geophys. Res.*, 115, D12113, doi:10.1029/2009JD012431.
- 23 Marshall, J. C., A. Adcroft, C. Hill, L. Perelman, and C. Heisey (1997a), A finite volume,
24 incompressible Navier-Stokes model for studies of the ocean on parallel computers, *J.*
25 *Geophys. Res.*, 102, 5753–5766.
- 26 Marshall, J. C., C. Hill, L. Perelman, and A. Adcroft (1997b), Hydrostatic, quasi-hydrostatic and
27 non-hydrostatic ocean modeling, *J. Geophys. Res.*, 102, 5733–5752.
- 28 McKinley, G. A., Fay, A. R., Takahashi, T., and Metzl, N. (2011), Convergence of atmospheric

1 and North Atlantic carbon dioxide trends on multidecadal timescales, *Nat. Geosci.*, 4, 606–
2 610, doi:10.1038/Ngeo1193.

3 McKinley, G. A., M. J. Follows, and J. Marshall (2004), Mechanisms of air-sea CO₂ flux
4 variability in the equatorial Pacific and the North Atlantic, *Global Biogeochem. Cycles*, 18,
5 GB2011, doi:10.1029/2003GB002179.

6 McKinley, G. A., T. Takahashi, E. Buitenhuis, F. Chai, J. R. Christian, S. C. Doney, M.-S. Jiang,
7 K. Lindsay, J. K. Moore, C. Le Quéré, I. Lima, R. Murtugudde, L. Shi, and P. Wetzel (2006),
8 North Pacific carbon cycle response to climate variability on seasonal to decadal timescales.
9 *J Geophys Res-Oceans*, **111**, C07S06, doi: 10.1029/2005JC003173.

10
11 Metzl, N., A. Corbière, G. Reverdin, A. Lenton, T. Takahashi, A. Olsen, T. Johannessen, D.
12 Pierrot, R. Wanninkhof, S. R. Ólafsdóttir, J. Olafsson, M. Ramonet (2010), Recent
13 acceleration of the sea surface *f*CO₂ growth rate in the North Atlantic subpolar gyre (1993–
14 2008) revealed by winter observations, *Global Biogeochem. Cycles*, 24, GB4004,
15 doi:10.1029/2009GB003658.

16
17 Mikaloff Fletcher, S. E., N. Gruber, A. R. Jacobson, M. Gloor, S. C. Doney, S. Dutkiewicz, M.
18 Gerber, M. Follows, F. Joos, K. Lindsay, D. Menemenlis, A. Mouchet, S. A. Müller, and J. L.
19 Sarmiento (2007), Inverse estimates of the oceanic sources and sinks of natural CO₂ and the
20 implied oceanic carbon transport, *Global Biogeochem. Cycles*, 21, GB1010,
21 doi:10.1029/2006GB002751.

22 Rayner, N. A., D. E. Parker, E. B. Horton, C. K. Folland, L. V. Alexander, D. P. Rowell, E.C.
23 Kent, and A. Kaplan (2003), Global analyses of sea surface temperature, sea ice, and night
24 marine air temperature since the late nineteenth century, *J. Geophys. Res.*, 108, 4407,
25 doi:10.1029/2002JD002670.

26 Sabine, C. L., R. A. Feely, N. Gruber, R. M. Key, K. Lee, J. L. Bullister, R. Wanninkhof, C. S.
27 Wong, D. W. R. Wallace, B. Tilbrook, F. J. Millero, T. Peng, A. Kozyr, T. Ono, A. F. Rios
28 (2004), The oceanic sink for anthropogenic CO₂, *Science* 305, 367–371.
29 doi: 10.1126/science.1097403.

- Schuster, U. G. A. McKinley, N. Bates, F. Chevallier, S. C. Doney, A. R. Fay, M. González-Dávila, N. Gruber, S. Jones, J. Krijnen, P. Landschützer, N. Lefèvre, M. Manizza, J. Mathis, N. Metzl, A. Olsen, A. F. Rios, C. Rödenbeck, J. M. Santana-Casiano, T. Takahashi, R. Wanninkhof, and A. J. Watson (2013), An Assessment of the Atlantic and Arctic sea-air- CO_2 fluxes, 1990-2009. *Biogeosciences*, 10, 607-627, doi:10.5194/bg-10-607-2013.
- Schuster, U., Watson, A.J., Bates, N., Corbière, A., González- Dávila, M., Metzl, N., Pierrot, D., and J. M. Santana-Casiano (2009), Trends in North Atlantic sea-surface fCO_2 from 1990 to 2006, *Deep Sea Res., Part II*, 56, 620–629, doi:10.1016/j.dsr2.2008.12.011.
- Séférián, R., Bopp, L., Swingedouw, D. and Servonnat, J. (2013), Dynamical and biogeochemical control on the decadal variability of ocean carbon fluxes. *Earth Syst. Dynam.* 4, 109–127, doi:10.5194/esd-4-109-2013.
- Takahashi, T., Sutherland, S. C., Wanninkhof, R., Sweeney, C., Feely, R. A., Chipman, D. W., Hales, B., Friederich, G., Chavez, F., Sabine, C., Watson, A., Bakker, D. C. E., Schuster, U., Metzl, N., Yoshikawa-Inoue, H., Ishii, M., Midorikawa, T., Nojiri, Y., Körtzinger, A., Steinhoff, T., Hoppema, M., Olafsson, J., Arnarson, T. S., Tilbrook, B., Johannessen, T., Olsen, A., Bellerby, R., Wong, C. S., Delille, B., Bates, N. R., and de Baar, H. J. W. (2009), Climatological mean and decadal change in surface ocean pCO_2 , and net sea-air CO_2 flux over the global oceans, *Deep-Sea Res. II*, 56, 554–577, doi:10.1016/j.dsr2.2008.12.009.
- Takahashi, T., Sutherland, S. C., Sweeney, C., Poisson, A., Metzl, N., Tilbrook, B., Bates, N., Wanninkhof, R., Feely, R. F., Sabine, C., Olafsson, J., and Nojiri, Y. (2002). Global sea-air CO_2 flux based on climatological surface ocean pCO_2 , and seasonal biological and temperature effects, *Deep-Sea Research II*, 49, 1601-1622.
- Terry, L. (2012), Evidence for multiple drivers of North Atlantic multi-decadal climate variability. *Geophys. Res. Lett.*, 39, L19712, doi:10.1029/2012GL053046.
- Thomas, H., F. Prowe, A.E., Lima, I.D., Doney, S.C., Wanninkhof, R., Greatbatch, R.J., Schuster, U., and A. Corbière (2008), Changes in the North Atlantic Oscillation influence CO_2 uptake in the North Atlantic over the past 2 decades, *Global Biogeochem. Cycles*, 22, doi: 10.1029/2007GB003167.

- 1 Thompson, D. & Wallace, J. M. (2000), Annular modes in the extratropical circulation. Part I:
2 Month-to-month variability. *J Climate*, **13**, 1000–1016.
- 3 Ullman, D.J., G.A. McKinley, V. Bennington, S. Dutkiewicz (2009), Trends in the North
4 Atlantic carbon sink: 1992-2006, *Global Biogeochem. Cycles*, 23, GB4011,
5 doi:10.1029/2008GB003383.
- 6
- 7 Von Storch, H. and F.W. Zwiers (1999) *Statistical Analysis in Climate Research*. Cambridge
8 University Press. 484 pp.
- 9 Wang, C., and S. Dong (2010), Is the basin-wide warming in the North Atlantic Ocean related to
10 atmospheric carbon dioxide and global warming?, *Geophys. Res. Lett.*, 37, L08707,
11 doi:10.1029/2010GL042743.
- 12 Watson, A. J., U. Schuster, D. C. E. Bakker, N. R. Bates, A. Corbière, M. González-Dávila, T.
13 Friedrich, J. Hauck, C. Heinze, T. Johannessen, A. Körtziner, N. Metzl, J. Olafsson, A. Olsen,
14 A. Oschlies, X. A. Padin, B. Pfeil, J. M. Santana-Casiano, T. Steinhoff, M. Telszewski, A. F.
15 Rios, D. W. R. Wallace and R. Wanninkhof (2009) Tracking the Variable North Atlantic
16 Sink for Atmospheric CO₂. *Science*, **326**, 1391–1393 DOI: 10.1126/science.1177394.
- 17 Williams, R. G., V. Roussenov, and M. J. Follows (2006), Induction of nutrients into the mixed
18 layer and maintenance of high latitude productivity, *Global Biogeochem. Cycles*, 20,
19 GB1016, doi:10.10292005GB002586.
- 20 Zhang, R. (2008), Coherent surface-subsurface fingerprint of the Atlantic meridional overturning
21 circulation. *Geophysical Research Letters*, **35**, L20705, doi:10.1029/2008GL035463.

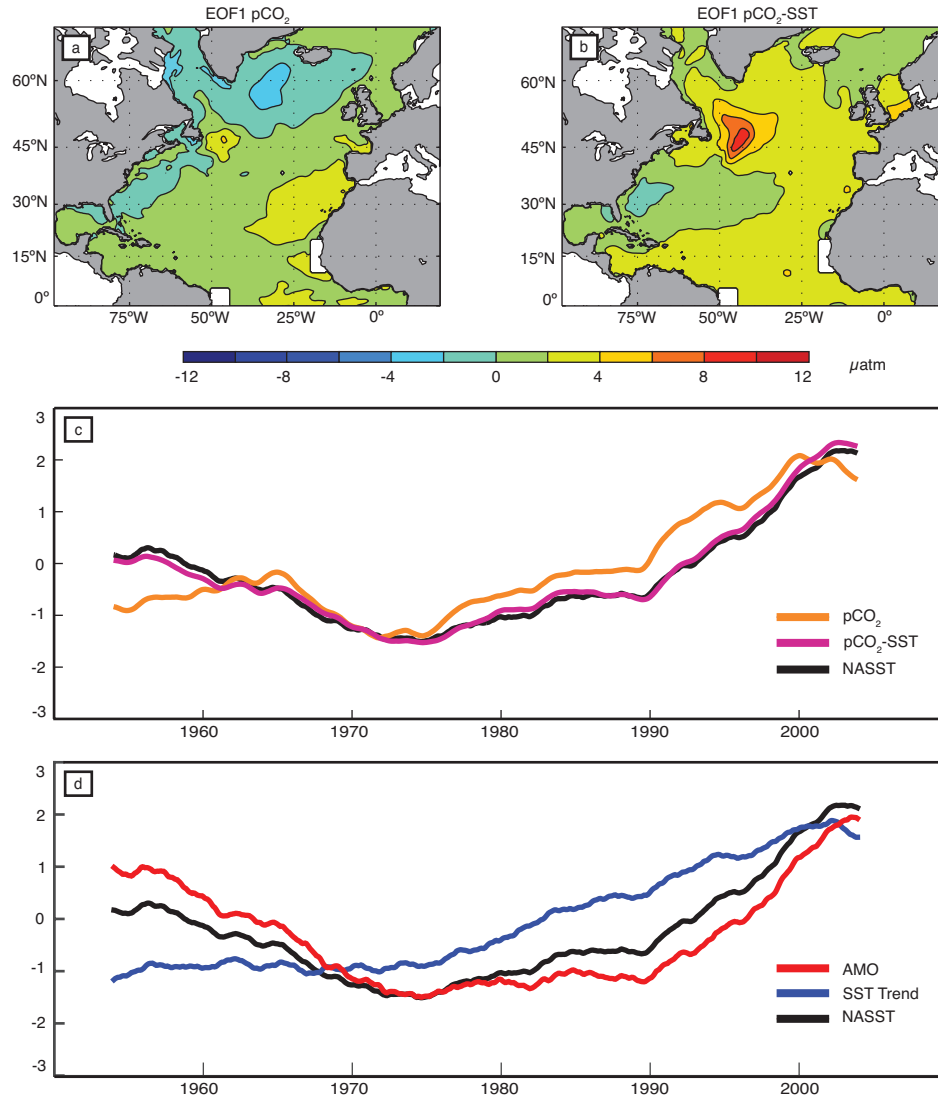


Figure 1: a) EOF1 of total pCO₂ (matm), b) EOF1 of pCO₂-SST (matm), explaining 18% and 38% of total variance, respectively. c) PC1- pCO₂ (orange), PC1- pCO₂-SST (pink) and area-weighted, basin-averaged standardized North Atlantic SST time series (black), d) Area-weighted, basin-averaged (0-70N, 98W-19.5E) North Atlantic SST from Had1SST (black), global area-weighted SST regressed onto North Atlantic SST (blue), and AMO index created by subtracting the global regression from the North Atlantic SST (red). All indices are standardized by 1-sigma. Timeseries smoothed with a 121-month box smoother. Two small coastal areas off Africa and South America were excluded in a) and b) due to the presence of localized, anomalously strong upwelling in the early 1960's that precluded elucidation of the large-scale pattern.

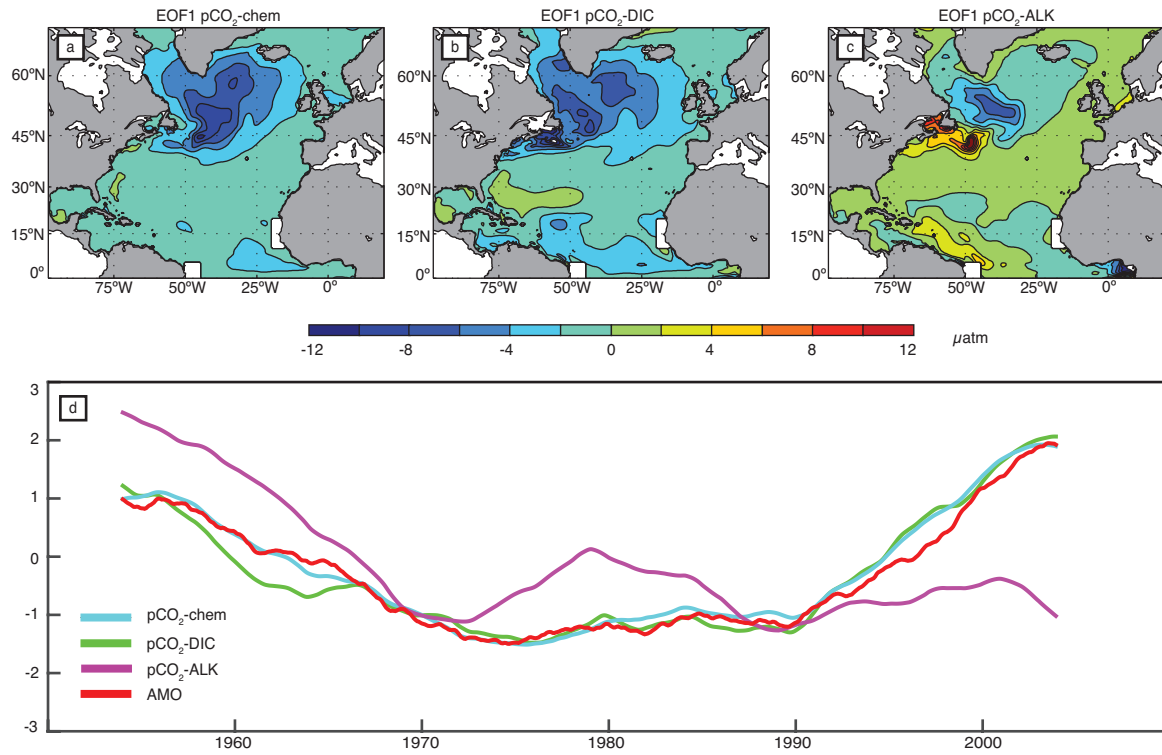


Figure 2: a) EOF1 pCO₂-chem (matm), b) EOF1 pCO₂-DIC (matm), c) EOF1 pCO₂-ALK explaining 32%, 25%, and 19% of total variance, respectively, d) PC1- pCO₂-chem (cyan), PC1- pCO₂-DIC (green) PC1-pCO₂-ALK (magenta) and AMO index (red), all standardized. Timeseries smoothed with a 121-month box smoother.

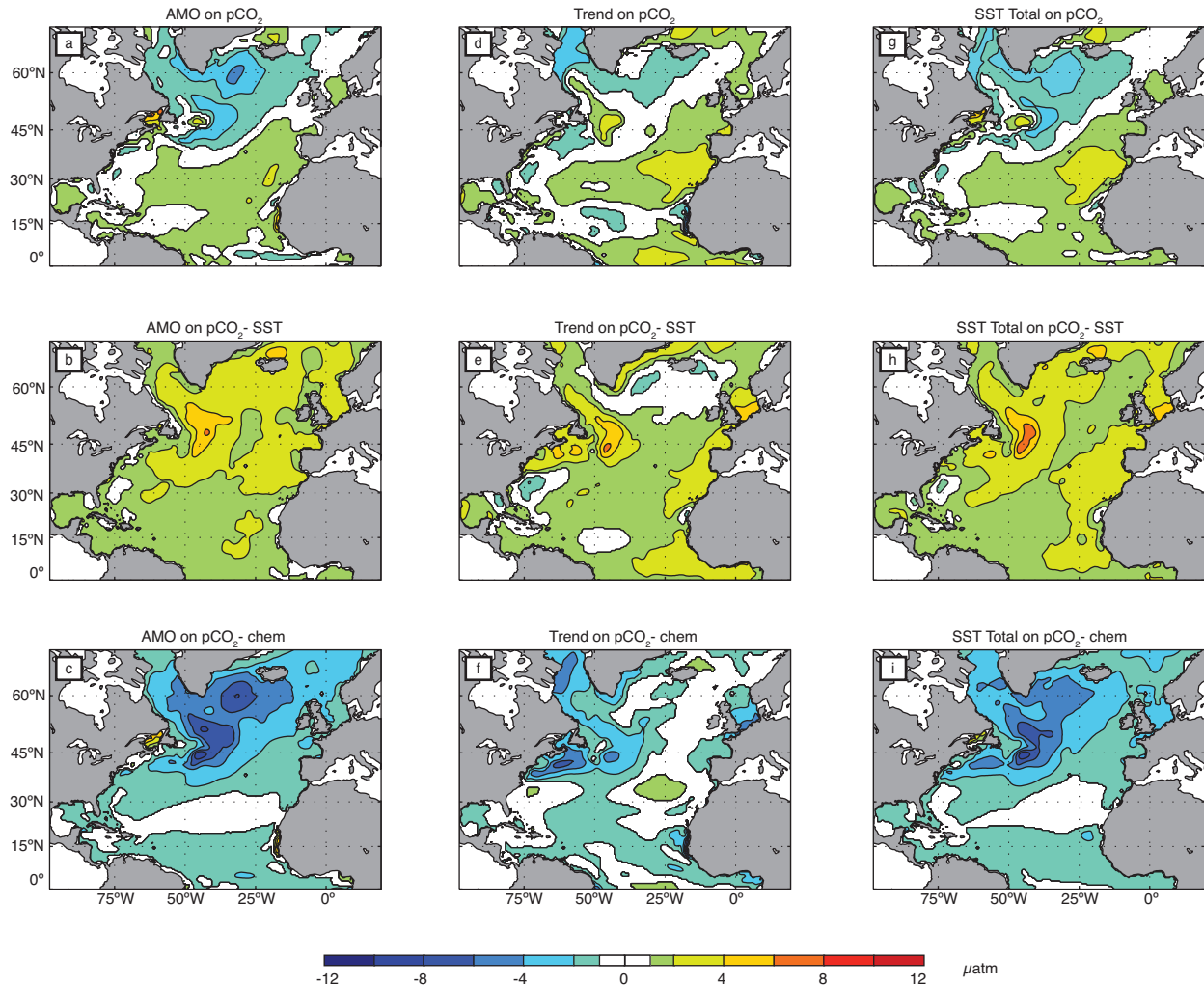


Figure 3: 121-month box-smoothed AMO regressed onto unsmoothed, monthly a) pCO₂, b) pCO₂-SST, c) pCO₂-chem. SST Trend regressed onto d) pCO₂, e) pCO₂-SST, f) pCO₂-chem. NASST (AMO + SST Trend) regressed onto g) pCO₂, h) pCO₂-SST, i) pCO₂-chem. Regressions calculated from 1953 through 2005. Values <0.5 and >-0.5 matm are whited out to highlight regions experiencing the most substantial changes.

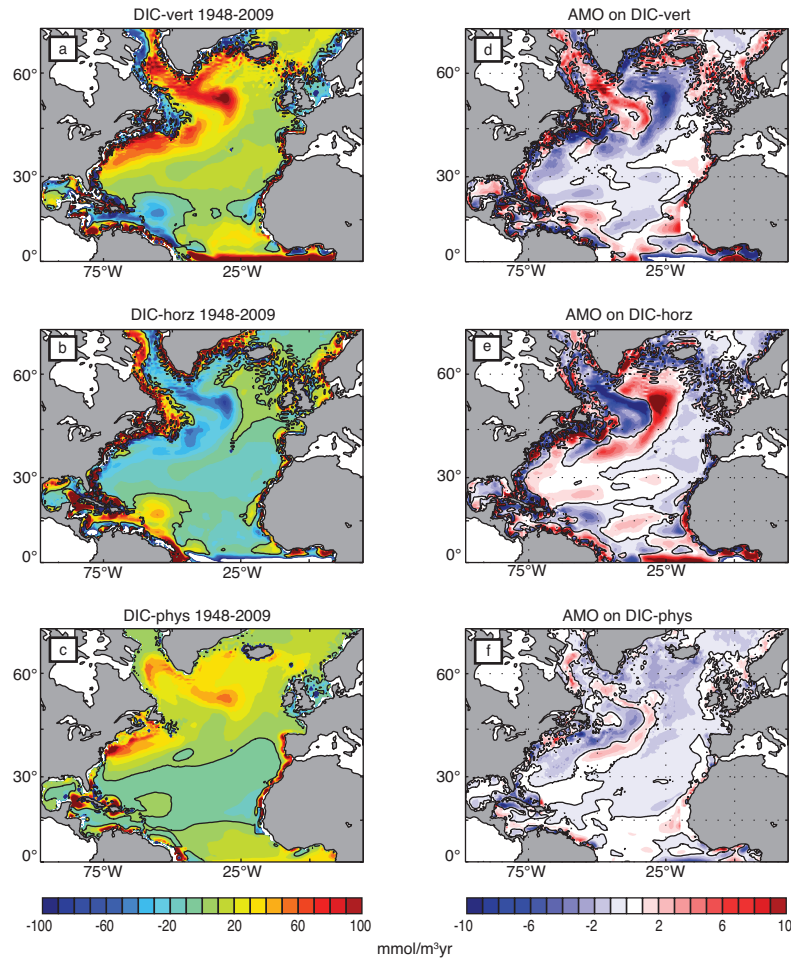


Figure 4: DIC diagnostics. Left column: 1948-2009 Mean a) DIC-vertical, b) DIC-horizontal, c) DIC-physical where DIC-physical is the sum of DIC-vertical and DIC-horizontal. Right column: AMO regressed onto d) DIC-vertical, e) DIC-horizontal, f) DIC-physical. Units mmol/ m³/yr.

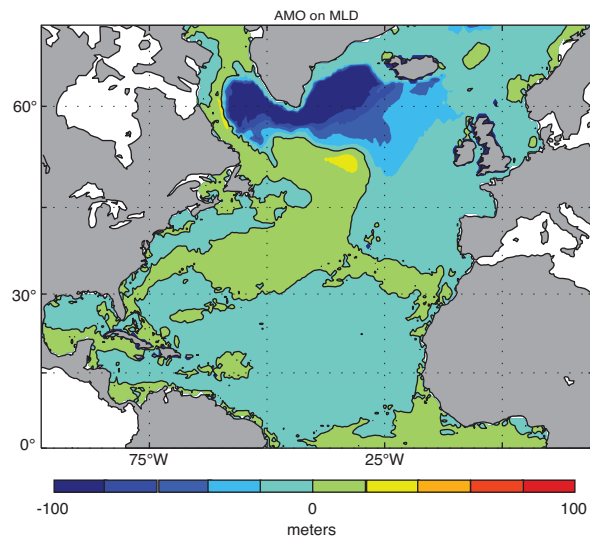


Figure 5: Regression of AMO on Mixed Layer Depth (MLD). Negative values denote a shoaling of MLD.

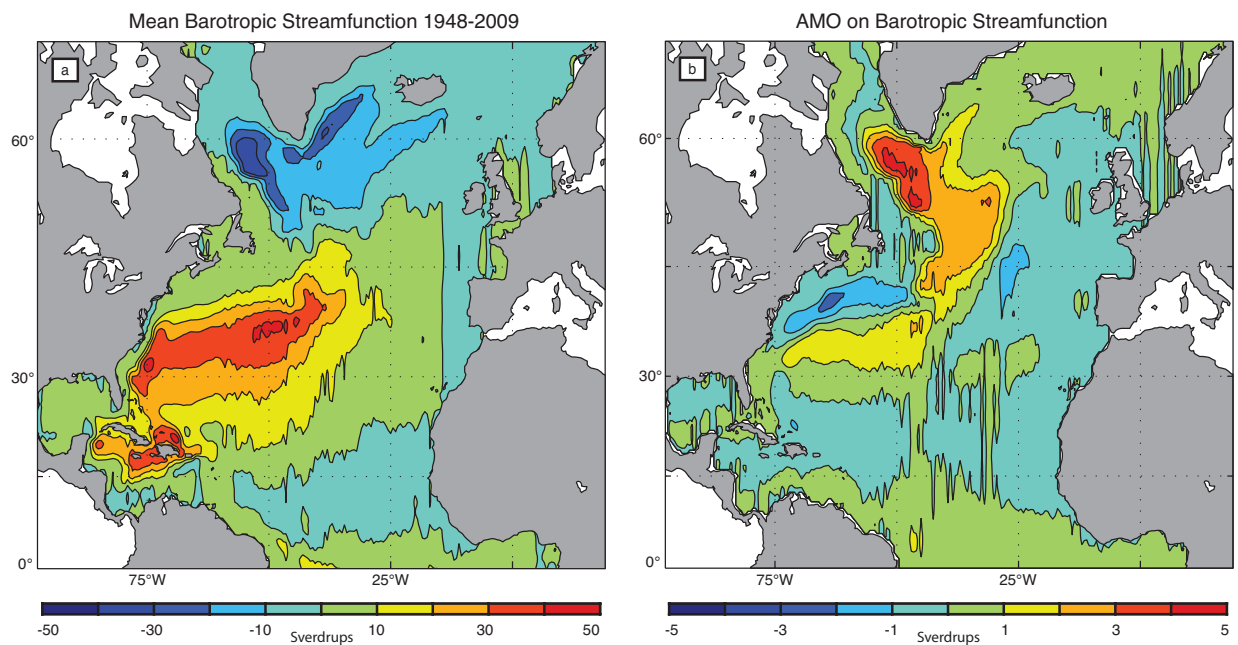


Figure 6: a) 1948-2009 mean barotropic streamfunction and b) AMO regressed onto barotropic streamfunction anomalies. Positive values denote clockwise motion. Units: Sverdrups ($1 \text{ Sv} = 10^6 \text{ m}^3 \text{ s}^{-1}$).

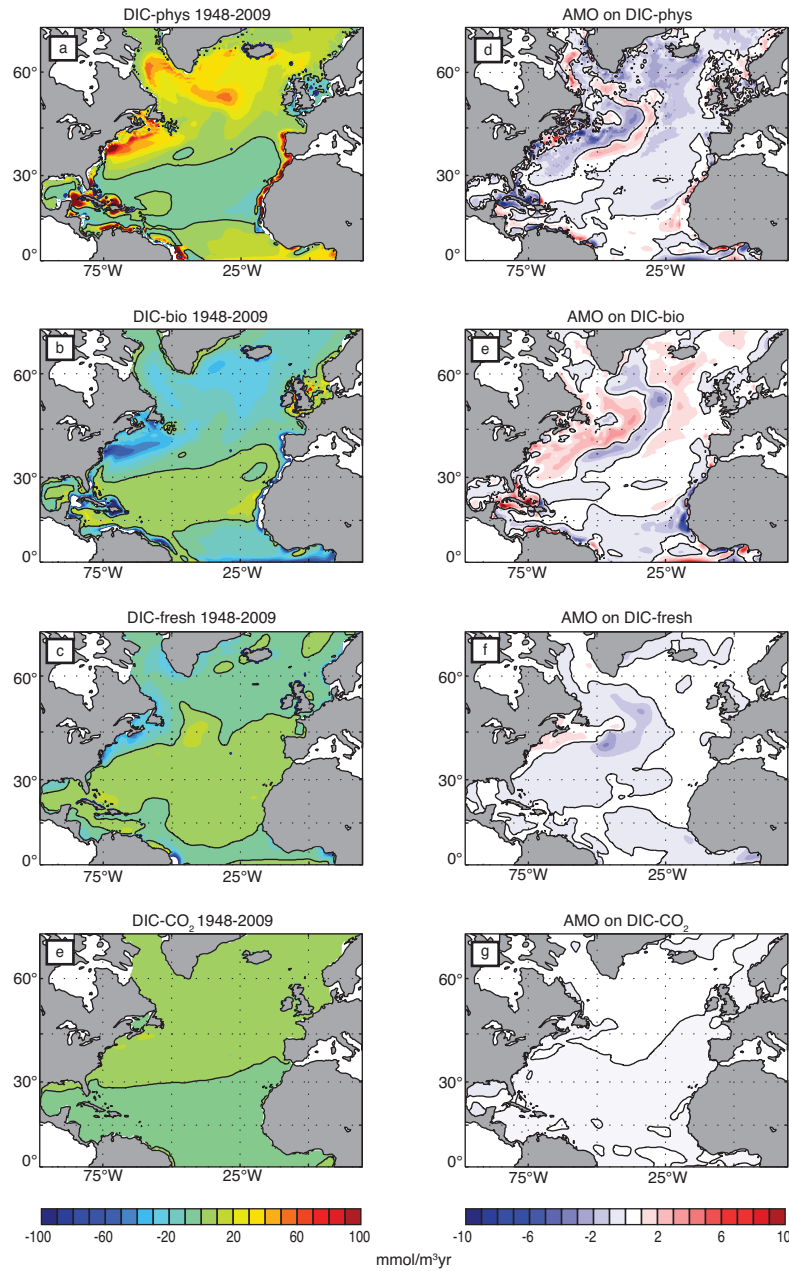


Figure 7: DIC diagnostics. Left column: 1948-2009 Mean a) DIC-physical, b) DIC-bio, c) DIC-fresh, d) DIC-CO₂ flux. Right column: AMO regressed onto e) DIC-physical, f) DIC-bio, g) DIC-fresh, h) DIC-CO₂ flux. Units mmol/m³/yr.